INSTRUMENTS AND METHODS OF INVESTIGATION PACS number: **29.20.–c**

Ion linear accelerators with high-frequency quadrupole focusing

Yu.A. Budanov, V.P. Golubkov, I.A. Grushichev, A.P. Maltsev, A.A. Timofeev, N.A. Chernyi

DOI: https://doi.org/10.3367/UFNe.2025.01.039854

Contents

Abstract. High-frequency quadrupole focusing (HFQF) has revolutionized ion linear accelerator technology. A brief historical essay on HFQF development is presented. Solutions to the problems undertaken at the Institute for High Energy Physics (IHEP) during the design work and fabrication of linear accelerators with HFQF are discussed. Spatially homogeneous quadrupole focusing (SHQF or, in Western terminology, RFQ) is now used in the front ends of almost all ion linear accelerators. A linear accelerator with spatially periodic quadrupole focusing (SPQF or, in Western terminology, RFQ DTL) is successfully operating as part of the IHEP accelerator complex. Spatially periodic quadrupole focusing has a number of advantages, both for proton acceleration and in heavy ion linear accelerators.

Keywords: ion linear accelerators, high frequency quadrupole focusing, fabrication and tuning technology

1. Introduction

Before the advent of high-frequency quadrupole focusing (HFQF), one of the bottlenecks for particle acceleration in linear resonant accelerators of ions was the entrance to the accelerator.

Yu.A. Budanov [(a)], **V.P. Golubkov** [(b)], **I.A. Grushichev** [(c)], **A.P. Maltsev** [(d)], **A.A. Timofeev** [(e)], **N.A. Chernyi** [(f)]
National Research Center Kurchatov Institute,
Institute for High Energy Physics,
pl. Nauki 1, 142281 Protvino, Moscow region, Russian Federation
E-mail: [(a)] Yury.Budanov@ihep.ru, [(b)] kernen2011@yandex.ru,
[(c)] Igor.Grushichev@ihep.ru, [(d)] Anatoliy.Maltsev@ihep.ru,
[(e)] Alexander.Timofeev@ihep.ru, [(f)] jird@yandex.ru

Received 15 November 2024, revised 24 January 2025
Uspekhi Fizicheskikh Nauk **195** (10) 1094 – 1107 (2025)
Translated by I.A. Ulitkin

This is where the particle velocity is lowest and the greatest difficulties arise in installing focusing magnetic lenses in drift tubes. Thus, high voltages were required at ion sources, and the RF-field wavelength in the resonators was increased.

The beam from the ion source was to be grouped into clusters to capture them for acceleration, which required the use of special devices. The percentage of particles captured for acceleration was approximately 60%.

A variation of HFQF — spatially homogeneous quadrupole focusing (SHQF or, in Western terminology, RFQ) — solved these problems. Spatially homogeneous quadrupole focusing made it possible to significantly reduce the injection energy, shorten the wavelength, and increase the capture efficiency to 100%.

High-frequency quadrupole focusing has two varieties: the aforementioned SHQF and spatially periodic quadrupole focusing (SPQF or, in Western terminology, RFQ DTL). Both focusing methods were offered at the Institute for High Energy Physics (IHEP) (the history of HFQF development is briefly described below).

Spatially homogeneous quadrupole focusing is now widely known and requires no special introduction. It is used in almost all ion linear accelerators designed to handle a vast range of charged particles, from protons to uranium ions.

Spatially periodic quadrupole focusing is successfully used in the URAL-30 proton linear accelerator with HFQF, which has been operating as an injector into the accelerator complex at the IHEP since 1985.

The technology for manufacturing SHQF accelerators is well-established. Accelerators with SPQF have also undergone their own evolution; however, publications on the technology for manufacturing such accelerators are scattered across preprints, reports, and journals and are not systematized. This technology still seems exotic.

In 2010, at the request of the Joint Institute for Nuclear Research (Dubna), researchers at the Institute for High Energy Physics designed a heavy ion linear accelerator with high-frequency quadrupole focusing (HILA with HFQF). It was considered to be an option for use as an injector for the NICA/MPD collider. This design proposed using SHQF and SPQF in the accelerator front end [or the so-called initial part of the accelerator (IPA)] and in its main part, respectively. The design parameters for this accelerator were published by Belyaev et al. [1]. The publication aroused great interest among experts in the field of accelerators and users of accelerated ions.

The problem is that, due to the low ion velocity, the efficiency of magnetic focusing in HILAs is low. Electrical focusing (HFQF is one of this type) is more effective. Spatially homogeneous quadrupole focusing is currently used in the front end of HILAs. However, magnetic lenses are still used in the main body. Despite the increased interest, no one has yet decided to use the SPQF in the main part of HILAs due to a lack of information on the manufacturing technology of such an accelerator.

There is a pressing need to systematize and review publications on the calculation, design, manufacture, and adjustment of this type of accelerator.

2. Brief historical overview

The idea of focusing particles using high-frequency quadrupoles has a long history. It was first put forward by V.V. Vladimirskii in 1956 [2]. He proposed producing a quadrupole component of the RF field in the accelerating gaps of the Alvarez accelerator using horns at the ends of drift tubes. However, this accelerator design proved ineffective.

Another method for producing a quadrupole component of the field in the accelerating gap was proposed in 1960 by G.M. Anisimov and V.A. Teplyakov [3], and independently by P. Lapostolle and F. Fer [4]. According to them, the quadrupole field is formed in the gaps between drift tubes with rectangular, mutually perpendicular apertures.

This focusing method was developed in more detail: methods for calculating focusing parameters were proposed [5, 6], and successful experiments on particle acceleration in model accelerators were performed [7, 8]. However, this type of focusing has fundamental drawbacks and can only be used in low-current accelerators.

More promising was high-frequency quadrupole focusing, proposed by V.A. Teplyakov in 1964, who suggested using horns in a so-called 'double' gap [9]. Here, an 'intermediate' electrode under an intermediate potential is placed in the gap between the drift tubes (between the 'main' or 'onboard' electrodes). Using this method, it was possible to achieve a high acceleration rate with an acceptable electric field strength at the horns by selecting the optimal parameters of the double gap [10]. The accelerating voltage between the electrodes was proposed to be generated in a cavity with a longitudinal magnetic field (in an H cavity [11]; see Section 4). For the same wavelength, the diameter of the H cavity is three-to-four times smaller than the diameter of the Alvarez cavity. An invertor's certificate was received for such an accelerator in 1967 [12].

The practical implementation of an accelerator with SPQF began at the IHEP in 1968 with the construction of a 4-MeV accelerator model [13]. Injection into this accelerator was carried out using a backup pre-injector of the IHEP I-100 linear accelerator. The accelerator was commissioned in 1971 [14].

The birth of the SHQF idea coincided precisely with the construction of the 4-MeV accelerator (1969). The basic principles of the theory were published by I.M. Kapchinskii and V.A. Teplyakov in their famous papers [15, 16]. A detailed development of the theory was presented in preprints [17, 18]. At the same time, a design for a 30-MeV proton linear accelerator with HFQF was proposed, consisting of a front end with SHQF and a main part with SPQF [19]. In 1969, V.V. Vladimirskii, I.M. Kapchinskii, and V.A. Teplyakov received an inventor's certificate for SHQF [20].

The SHQF accelerator as an independent facility was put into operation in 1972 [21]. Despite the fact that all the ideas were published, SHQF accelerators were developed at the IHEP alone for seven years. Only in 1976–1977 was the idea of SHQF put into practice at the Institute of Theoretical and Experimental Physics (Soviet Union) [22] and Los Alamos (United States) [23]. Following this, SHQF accelerators or, in Western terminology, RFQ linacs, gained widespread popularity. In 1988, I.M. Kapchinskii and V.A. Teplyakov were awarded the Lenin Prize and the American Physical Society Prize for their invention of SHQF.

In 1973, a design was developed for a proton linear accelerator with HFQF (URAL-30) as an injector for the U-70 proton synchrotron booster [24]. The URAL-30 accelerator was manufactured entirely in the IHEP workshops, demonstrating its technological feasibility.

The first part of the accelerator (up to 16 MeV) was put into operation in 1975 [25], and the physical start-up of the entire accelerator took place in 1977 [26]. For several years, the accelerator was used as a mockup to study the features of a new type of accelerator and to identify and eliminate weak points in its design.

Using the data obtained, the accelerator channel was recalculated for a lower field strength. After the completion of the booster building, the URAL-30 accelerator was installed and commissioned for booster adjustment (1983). Since 1985, the URAL-30 accelerator has been operating at the IHEP accelerator complex as an injector in the booster. The calculated parameters of URAL-30 are given in [27], and the experimental parameters are presented in [28–31].

Currently, a new accelerator with HFQF, URAL-30M, has been manufactured at the IHEP to replace the physically obsolete URAL-30 accelerator [32]. In addition, several more linear accelerators with HFQF have been built at the IHEP for research purposes and on orders from third-party organizations.

3. A few words about accelerators with spatially homogeneous quadrupole focusing, developed at Institute for High Energy Physics

The use of SHQF at the front end of ion linear accelerators has long been routine. All the key concepts used to form particle bunches in SHQF-based accelerators, now considered classical, were first tested at the IHEP. They include focusing and accelerating particles in the channel of a modulated four-wire line, adiabatic particle bunching, acceleration with a constant equilibrium phase, and high-frequency beam matching at the channel entrance. The results of numerical and field experiments conducted during the development of SHQF were published in the abovementioned preprints, reports, and papers.

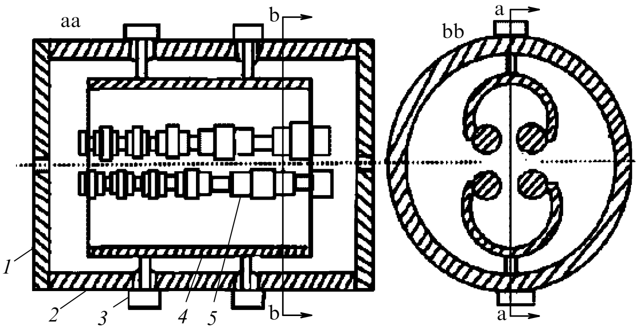

Figure 1. Schematic of 2H cavity: *1* — flange, *2* — container, *3* — cavity mounting unit, *4* — cavity, and *5* — accelerating electrode.

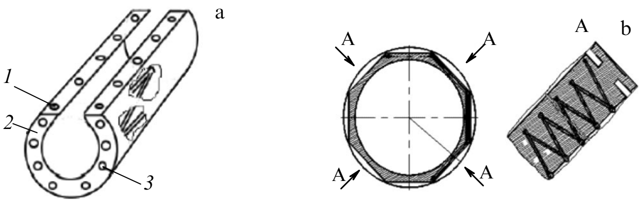

Figure 2. (a) Sketch of SHQF cavity with cooling channels: *1* — holes for mounting electrodes, *2* — cavity end face, and *3* — welded channel outputs; (b) location of cooling channels in container body.

The most commonly used accelerating system for RFQ in the world is a four-chamber cavity (4Ch cavity). This type of cavity was proposed at the IHEP [15], but, in SHQF-based accelerators built at the IHEP, preference was given to a 2H cavity [17, 36]. A schematic of one of the first 2H cavities is shown in Fig. 1.

The advantage of the 2H cavity is that its nearest parasitic oscillation mode is far removed in frequency from the working mode. This ensures its manufacturability and ease of tuning.

The first 2H cavities were made of steel. The working surfaces were coated with 100-μm-thick galvanic copper. Cooling channels with a corrosion inhibitor were drilled into the cavity body.

Subsequently, aluminum alloy grade AMg-6, which is corrosion resistant and light, as well as having high thermal conductivity and good processing properties, was used instead of steel for HFQF containers and cavities. Semi-finished thick-walled tubes made of AMg-6, the diameters of which are close to the required dimensions, were employed to manufacture the cavities and containers. To cool them, a technology was developed for oblique counter-drilling of channels in the cavity (container) body using an auger drill with a working length of ~ 400 mm and for sealing the external holes using friction welding (Fig. 2).

The technology for manufacturing accelerating electrodes for SHQF-based accelerators is constantly being improved. The very first accelerating electrodes were manufactured on lathes. They were shaped like rotating bodies, with diameters modulated either along a staircase pattern (see Fig. 1) or with conical transitions (Fig. 3a). Later, blade-shaped electrodes (Fig. 3b) were manufactured on computer-controlled machines [37, 38].

In all cases, the electrode material was oxygen-free copper (Mob grade). Several accelerators with SHQF were built for research purposes at the IHEP.

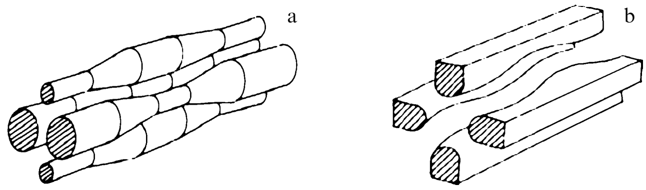

Figure 3. SHQF accelerating electrodes: (a) with conical transitions and (b) in the form of blades.

Parameter and Unit of Measurement	URAL-30	URAL-30M	NICA
Accelerated ion type	H^+	H^+	Au_{197}^{31+}
Charge-to-mass ratio	1	1	0.157
Injection energy W_{in}, keV/u	100	100	32.5
Output energy W_{out}, keV/u	1980	1770	407.1
Design current I, mA	100	100	5–10
Energy spectrum width, %	3	8.8	7.6
Bunch phase width, deg	45	28	99
Normalized beam emittance, π, mrad cm	0.18	0.14	0.08
Cavity voltage U, kV	150	140	96
Maximum electrode field strength E_{max}, kV cm^{-1}	225	250	207
Section length L, mm	4052	2461	6915
Average channel radius R_0, mm	8.82	7.59	6.4

The proton beam dynamics were studied using the initial part of the accelerator, IPA2-E ($W_{in} = 0.1$ MeV, $W_{out} = 2$ MeV, $F = 148.5$ MHz, $I_{max} = 250$ mA, $L \cong 4$ m, and a duty cycle of 1000).

Design solutions for fabricating an SHQF-based accelerator with a low-duty cycle were tested at the HILA facility (a duty cycle of 100, $F = 148.5$ MHz, $W_{in} = 0.1$ MeV, $W_{out} = 10$ MeV, and $I_{max} = 100$ mA). An SHQF-based accelerator ($W_{out} = 2$ MeV) was part of the HILA facility.

A transportable SHQF-based accelerator was manufactured: a demonstration accelerator (DA) operating at a frequency of 151 MHz with an output energy of 1 MeV (protons). This accelerator was self-contained in terms of RF power supply, vacuum, and cooling. The RF power supply was configured as a self-generating generator. Only connections to the power grid and water supply were needed.

In the accelerators with SHQF discussed in this paper, the SHQF sections are integral components. The main parameters of these sections are listed in the table.

4. Methods for calculating parameters of spatially periodic quadrupole focusing

As high-frequency quadrupole focusing developed, methods for calculating its parameters improved. In the pre-computer era, when the idea of high-frequency quadrupole focusing was put forward, only analytical methods were available.

The task of calculating high-frequency quadrupole focusing parameters was not a simple one. During the acceleration period (in the double gap, Fig. 4), the focusing and acceleration parameters depend on many factors: the aper-

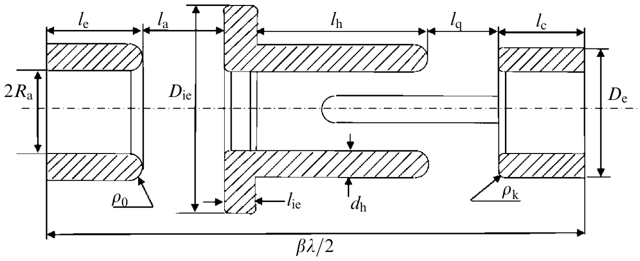

Figure 4. Schematic of acceleration period in regular part of channel: $2R_a$ is aperture diameter, D_{ie} is outer diameter of intermediate electrode, D_e is outer diameter of board electrode, d_h is horn diameter, ρ_0 is radius of board electrode output end, ρ_k is radius of electrode edges, $\beta\lambda/2$ is acceleration period length, l_e is half the board electrode length, l_a is length of axially symmetric gap, l_{ie} is length of intermediate electrode, l_h is horn length, and l_q is length of gap between horn end and end of adjacent electrode.

ture radius; the lengths of the gaps, horns, and electrodes; the voltage division by the halves of the double gap; the horn diameters; and the radii of the electrode edges.

To calculate the focusing parameters, boundary conditions on the aperture generatrix were required, but they were not known. Using the assumption that, at the aperture boundary, at azimuths corresponding to the horn axes, the longitudinal component of the electric field can be approximated by a square wave, the problem of selecting the optimal double gap was solved in a very general form [10]. Calculation formulas and diagrams were constructed, which were used to calculate a 4-MeV accelerator model [13].

Subsequently, a method for determining the boundary conditions in the double gap was developed using measurements in an electrolytic bath [39]. (The URAL-30 accelerator was initially designed using this method.) Measurements in an electrolytic bath made it possible to obtain accurate data on the boundary conditions at the aperture boundary; however, they were labor-intensive and slow when selecting the channel design. Therefore, efforts were made to develop a program for calculating boundary conditions on a computer.

A fairly effective method for calculating boundary conditions was developed using the eigenfunction method in combination with the Monte Carlo method [40]. Determining the potential at individual points eliminates the need to solve the problem for the entire domain, significantly reducing RAM consumption, the small capacity of which was the main limitation of computers at the time. The channel for the URAL-30 accelerator was already recalculated using this method, and the URAL-30M accelerator was calculated using it from the very beginning. This method was used at the IHEP for quite a long time to solve many problems.

Let us discuss the procedure for calculating the focusing and acceleration parameters in a channel with SPQF. The high-frequency field inside the channel aperture in the electrostatic approximation is written in the form of a Fourier–Bessel series:

$$U(r,\theta,z) = \sum_{n=0,\,m=1}^{\infty} \cos(2n\theta)\, I_{2n}(mkr) \times \left[a_{2n,m}\sin(mkz) + b_{2n,m}\cos(mkz)\right]. \quad (1)$$

Here, (r,θ,z) are the coordinates of the points in the cylindrical system, $k = 2\pi/\beta\lambda$, $I_{2n}(mkr)$ are the modified Bessel functions, β is the relative velocity, λ is the wavelength, and the voltage over the acceleration period $\beta\lambda/2$ is assumed to be unity. The potential values at the $\beta\lambda/2$ period electrodes continue in accordance with the sequence of switching the main (board) electrodes from one side of the cavity to the other.

The main azimuthal harmonics of the field are the accelerating axially symmetric ($n = 0$) and focusing quadrupole ($n = 1$) harmonics. Higher azimuthal harmonics are minimized by selecting the horn diameter. (For example, the most significant harmonic from the standpoint of field nonlinearity, $n = 3$, is zero if the angle at which the horn diameter is visible from the channel axis is 60° [41].)

In the presence of boundary conditions $U(R_a, 0, z)$ and $U(R_a, \pi/2, z)$, the accelerating and focusing harmonics of the field are calculated using the formulas

$$\begin{pmatrix} a_{0,m} \\ b_{0,m} \end{pmatrix} = \frac{1}{\beta\lambda I_0(mkR_a)} \int_0^{\beta\lambda} \left[U(R_a,0,z) + U\left(R_a, \frac{\pi}{2}, z\right)\right] \times \begin{pmatrix} \sin(mkz) \\ \cos(mkz) \end{pmatrix} \mathrm{d}z\,, \quad (2)$$

$$\begin{pmatrix} a_{2,m} \\ b_{2,m} \end{pmatrix} = \frac{1}{\beta\lambda I_2(mkR_a)} \int_0^{\beta\lambda} \left[U(R_a,0,z) + U\left(R_a, \frac{\pi}{2}, z\right)\right] \times \begin{pmatrix} \sin(mkz) \\ \cos(mkz) \end{pmatrix} \mathrm{d}z\,. \quad (3)$$

After calculating the harmonics, the z dependence of the electric field strength at the channel axis,

$$E_z(0,0,z) = -\sum_{m=1}^{\infty} (mk)\left[a_{0,m}\cos(mkz) - b_{0,m}\sin(mkz)\right], \quad (4)$$

and the acceleration efficiency,

$$\vartheta = \frac{1}{U}\int_0^{\beta\lambda/2} E_z(0,0,z)\cos(kz)\,\mathrm{d}z\,, \quad (5)$$

are computed. The position of the electrical center of the acceleration period is determined from the condition

$$\int_0^{\beta\lambda/2} E_z(0,0,z)\sin(kz)\,\mathrm{d}z = 0\,. \quad (6)$$

Transverse oscillations of particles in an accelerator are described by the equation

$$\mathrm{d}^2\begin{pmatrix} x \\ y \end{pmatrix} / \mathrm{d}t^2 = \frac{e}{2m_0\gamma^3}\left(-\frac{\partial E_z}{\partial z} \pm \left(\frac{\partial E_x}{\partial x} - \frac{\partial E_y}{\partial y}\right)\right) \times \cos(kz+\varphi)\begin{pmatrix} x \\ y \end{pmatrix}. \quad (7)$$

Here, $\varphi = \omega t$, ω is the angular frequency of the RF field, t is the time, m_0 is the rest mass of a particle, e is the particle charge, and $\gamma = 1/[1-\beta^2]^{1/2}$. The available harmonics allow one to calculate the gradients of the field strength components:

$$\frac{\partial E_z}{\partial z} = \sum_{m=1}^{\infty} (mk)^2\left[a_{0,m}\sin(mkz) + b_{0,m}\cos(mkz)\right], \quad (8)$$

$$\frac{\partial E_x}{\partial x} - \frac{\partial E_y}{\partial y} = -\sum_{m=1}^{\infty} 0.5(mk)^2\left[a_{2,m}\sin(mkz) + b_{2,m}\cos(mkz)\right]. \quad (9)$$

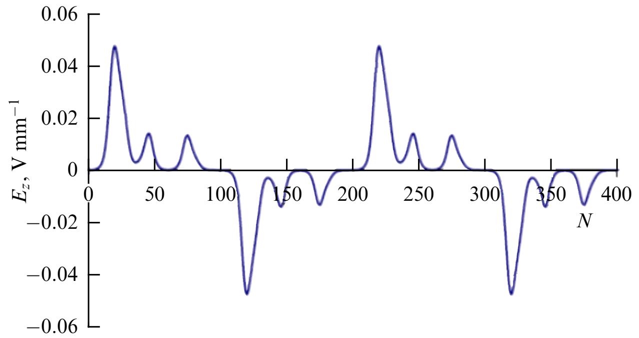

Figure 5. Distribution of longitudinal accelerating component of electric field on channel axis during focusing period.

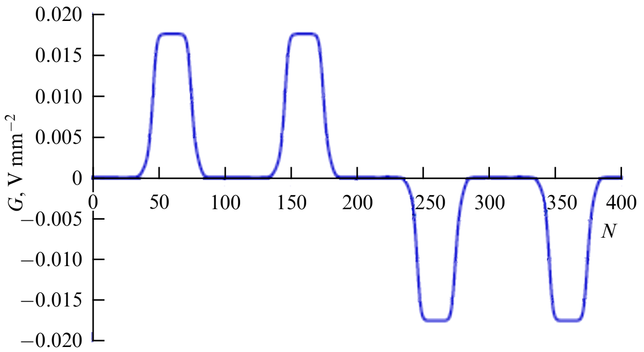

Figure 6. Distribution of gradient of transverse focusing components of electric field strength during focusing period.

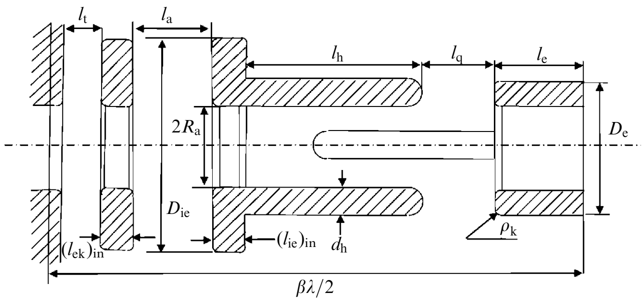

Figure 7. Input acceleration period: $(l_{ie})_{in}$ is length of input intermediate electrode, $(l_{ek})_{in}$ is length of screen electrode, and l_t is end drift length.

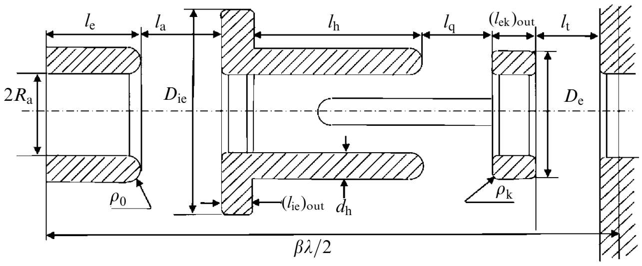

Figure 8. Output acceleration period: $(l_{ie})_{out}$ is length of output intermediate electrode, $(l_{ek})_{out}$ is length of screen electrode, and l_t is end drift length.

Practice has shown that 128 harmonics are sufficient for a satisfactory calculation of the field components. Figures 5 and 6 show an example of the z-distribution of the accelerating field component and the gradient of the focusing components for one of the FFDD focusing periods. Here, $E_z \equiv -\partial U/\partial z$, $G \equiv \partial E_x/\partial x - \partial E_y/\partial y$, and N is the number of the period split point.

The main physical parameters determining transverse motion are the phase shift of the transverse oscillations during the focusing period μ and the instantaneous oscillation frequencies — the minimum frequency $\nu_{\min}$ and the maximum frequency $\nu_{\max}$. The channel acceptance depends on the minimum frequency:

$$A = \nu_{\min} R_a^2 \frac{\gamma}{N_f \lambda}\,. \qquad (10)$$

Here, N_f is the number of periods $\beta\lambda$ during the focusing period.

The ratio $\nu_{\min}/\nu_{\max}$ of the frequencies determines the ratio of the beam semiaxes:

$$\frac{x_{\min}}{x_{\max}} = \sqrt{\frac{\nu_{\min}}{\nu_{\max}}}\,. \qquad (11)$$

A matrix method is used to calculate μ, $\nu_{\min}$, and $\nu_{\max}$. The focusing period ($2\beta\lambda$) is divided into a sufficiently large number of intervals (usually 400), so that each one can be considered a thin lens with a matrix in the form of a product of the matrices of the refractive plane and the drift region:

$$\begin{bmatrix} x \\ \mathrm{d}x/\mathrm{d}z \end{bmatrix} = \begin{bmatrix} 1 & l \\ 0 & 1 \end{bmatrix} \begin{bmatrix} 1 & 0 \\ a & 1 \end{bmatrix} \begin{bmatrix} x \\ \mathrm{d}x/\mathrm{d}z \end{bmatrix}_0 . \qquad (12)$$

Here, l is the drift length, $a = -e(E_{zz} \pm G)\cos(kz + \varphi)/(2m_0c^2\beta^2\gamma^3)$, $E_{zz} \equiv \partial E_z/\partial z$.

By multiplying the focusing period matrices, we find

$$\cos\mu = 0.5(M_{11} + M_{22})\,, \quad \nu_{\min} = \sqrt{\frac{M_{21}}{M_{12}}}\,, \qquad (13)$$

where M_{ik} are the matrix elements of the resulting matrix.

To find $\nu_{\max}$, we simply need to change the sign of the gradient G. Expression (13) for $\nu_{\min}$ and $\nu_{\max}$ is valid provided that the beginning of the focusing period ($z = 0$) is at the extremum point of the envelope (for FFDD focusing, it is in the middle of two equally focusing acceleration periods).

Input and output channel periods differ in their structure from the periods of the regular part (Figs 7 and 8).

In the input period, a shielding electrode at zero potential (at the end flange potential) is installed between the cavity end wall and the intermediate electrode. In the output period, the role of the shielding electrode is played by the board electrode, disconnected from the side and connected to the cavity at a point with zero potential. The calculation of the input and output periods is similar to the described procedure, but, to find the boundary conditions, the program must be adjusted accordingly, taking into account the above-mentioned features of these periods.

The procedure for calculating the geometry of a channel with SHQF is briefly described in [1]. When selecting the physical parameters of a linear accelerator, many different (sometimes contradictory) requirements and constraints must be taken into account. In the case of HFQF, one of the most important constraints is related to the selection of the maximum permissible field strength on the surface of the accelerating electrodes.

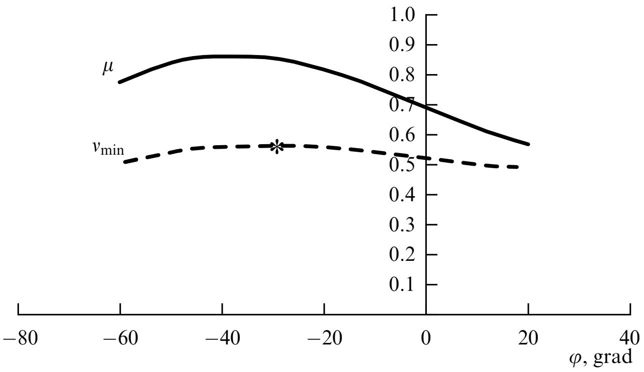

Figure 9. Dependences of $\nu_{\min}(\varphi)$ and $\mu(\varphi)$ on phase in first section of HILA with HFQF.

Many years of practical experience at the IHEP show that, in an accelerator with SPQF, the maximum field strength $E_{\max}$ at the accelerating electrodes can reach $2.9E_{\mathrm{K}}$ [41], where E_{K} is Kilpatrick's criterion [42]. At the same time, accelerator operation remains stable, and the percentage of failures caused by cavity breakdowns does not exceed 0.02%. Moreover, due to the low stored energy in the cavities, sparking between the electrodes does not damage their surfaces but cleans them of contaminants, i.e., training occurs.

The choice of acceleration and focusing channel parameters determines both the accelerator performance and the quality of the accelerated particle beam. Bunch formation does not terminate in SHQF. It continues for some time in the main part of the accelerator and affects the beam quality, in particular, the magnitude of its emittance.

In HILAs with magnetic focusing, particle defocusing by the accelerating RF field depends on the field phase, while focusing by magnetic lenses is independent of the phase. This leads to a phase dependence of the oscillation frequencies $\nu_{\min}$, $\nu_{\max}$, and μ and to an increase in beam emittance. In HILAs with HFQF, focusing is phase dependent, and by selecting the geometry of the double gap, this dependence can be significantly weakened and an increase in emittance can be reduced. As an example, Fig. 9 shows the dependences of $\nu_{\min}$ and μ on the phase φ in the main part of the HILA for one of the designs developed at the IHEP.

The asterisk in the figure indicates the value of $\nu_{\min}$ for the equilibrium phase $\varphi_s = -30°$. It is easy to see that, in the range of operating phases ($\Delta\varphi \approx 80°$), the minimal frequency dependence on phase is ensured.

The scope of this review does not allow a detailed discussion of this important issue; a more comprehensive paper is needed here.

5. Accelerating systems

At the IHEP, cavities with a longitudinal magnetic field, shown in Fig. 10, were used as accelerating systems for SPQF.

The first of these to be developed was the H cavity.

5.1 H cavity

The H cavity consists of two tubes inserted one inside the other. The larger-diameter and longer tube is closed at the ends by caps and serves as a container. The inner tube does not touch the bottoms. A slit is cut along the generatrix of this tube, creating a potential difference in the electric field component when electromagnetic oscillations with a longitudinal magnetic field are excited in the cavity.

Let us briefly discuss the problems that arose during the development of the H cavity and the methods to solve them. Similar problems encountered during the development of other cavities were solved based on the experience gained.

The first problem was to estimate the radiotechnical parameters of the H cavity based on its geometric dimensions. Teplyakov and Stepanov [11] made an attempt to assess its basic parameters (the fundamental oscillation frequency and RF power loss) by stitching the solutions of Maxwell's equations in different regions of the H cavity.

However, the geometry of the H cavity is too complex for analytical estimates: the cavity has end regions, and accelerating electrodes are installed inside the slit. Therefore, despite numerous attempts, analytical methods proved insufficiently accurate, and computers at that time were underpowered. As a result, experiments on prototypes became the primary method for studying cavities during the development of SPQF-based accelerators [43, 44].

A prototype H cavity was developed that allows such experiments to be performed. The influence of the end regions on the resonant frequency and field distribution along the experimental section of the cavity was eliminated by installing 'shielding' turns in the end regions. The resulting section simulated an infinitely long H cavity in terms of frequency and field distribution. It was used to study the dependence of the cavity capacitive loading on the geometric dimensions of the electrodes and to refine the resonator diameter for the selected operating frequency.

In the H cavity, intermediate electrodes are installed in the inner tube along a generatrix that is diametrically opposite the gap. When the capacitances of both halves of the gap are equal, the current in the intermediate electrode leg is zero, and the cavity Q factor is maximal. However, these capacitances should be equalized.

In the 4-MeV accelerator model, equality of capacitances was achieved by adjusting the outer diameters of the

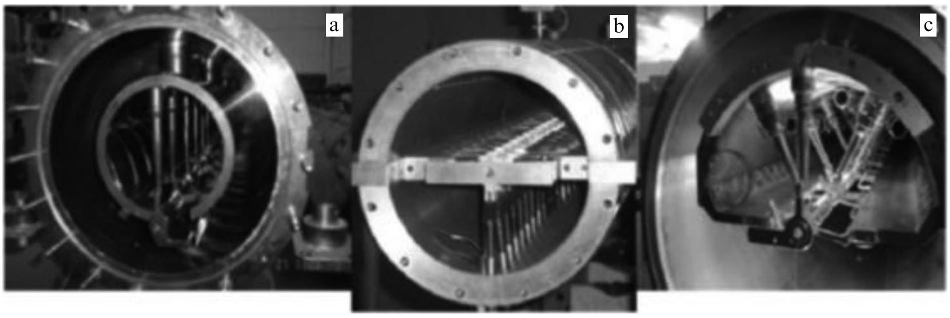

Figure 10. Cross sections of cavities with longitudinal magnetic field: (a) H cavity, (b) 2Ch cavity, and (c) SH cavity.

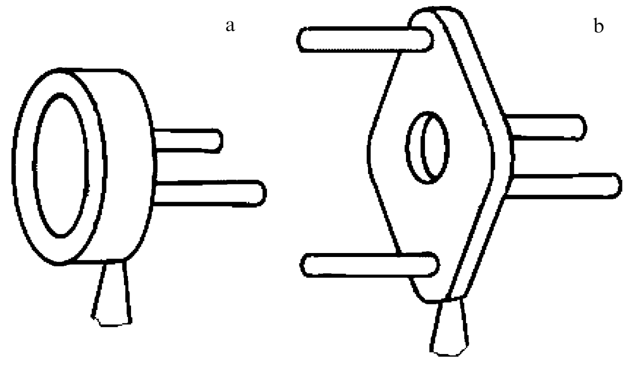

Figure 11. Intermediate electrode with (a) cup and (b) balancing horns.

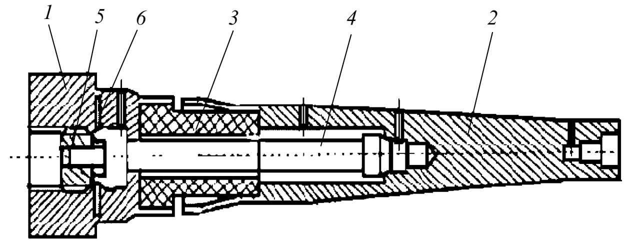

Figure 12. Sketch of intermediate electrode leg with shielded resistor: *1* — leg base, *2* — leg body, *3* — ceramic bushing, *4* — wire resistor, *5* — clamping screw, and *6* — contact collet.

electrodes. Disadvantages of this method are obvious, and other capacitive balancing methods were subsequently tested. In the URAL-30 accelerator, use was made of balancing by a 'cup' on the intermediate electrode (Fig. 11a), sliding from the outside onto the board electrode. However, this scenario is inconvenient for electrode installation. Furthermore, a secondary resonance discharge could be generated within the cup. Therefore, during final installation of the URAL-30 accelerator, the cup was replaced with balancing horns located away from the axis (Fig. 11b).

In the H cavity, even precise balancing of the aforementioned capacitors may result in parasitic resonance (or 'leg resonance'), leading to voltage imbalance in the gaps. To prevent this, resistors of approximately $\sim 100\ \Omega$ were inserted into the intermediate electrode legs. The first versions of these resistors were made of refractory sealing mastic (MOU brand). These resistors quickly burned out and were replaced with wire-wound does, wound from refractory wire (nichrome) on a ceramic insert. However, these resistors could not withstand interturn breakdowns that occurred during breakdowns in the gaps between the electrodes. Furthermore, the presence of a wire-wound resistor at the maximum of the magnetic field of the cavity leads to increased RF power losses.

In an improved design of the intermediate leg, this resistor is protected from the cavity's alternating magnetic field by a metal shield (Fig. 12).

The base of leg *1* is connected to housing *2* via ceramic sleeve *3*, which houses a wire resistor *4*, secured with a clamping screw and washers (*5* and *6*). A gap approximately 1 mm in width between the shield and the leg base acts as a spark gap, shunting the resistor during breakdown.

Introducing a resistor into the intermediate electrode leg is not the only way to avoid leg resonance. A leg design with capacitive reactance, in which the resonant frequency of the leg is always higher than the operating oscillation frequency, is considered in [45]. This leg allows water cooling and may be of interest for HFQF-based accelerators operating in a low-duty-cycle regime.

The next important issue is the tuning of the field distribution along the cavity. This is accomplished using additional capacitive elements installed on the sides of the cavity, or using inductive elements in the magnetic field, as well as by adjusting the size of the end sections. The cavity frequency is simultaneously tuned to precisely match the RF generator frequency. To fine-tune the frequency, an automatic frequency control system was developed, comprising rotating rings located in the magnetic field, an error signal processing unit, and actuators (Fig. 13).

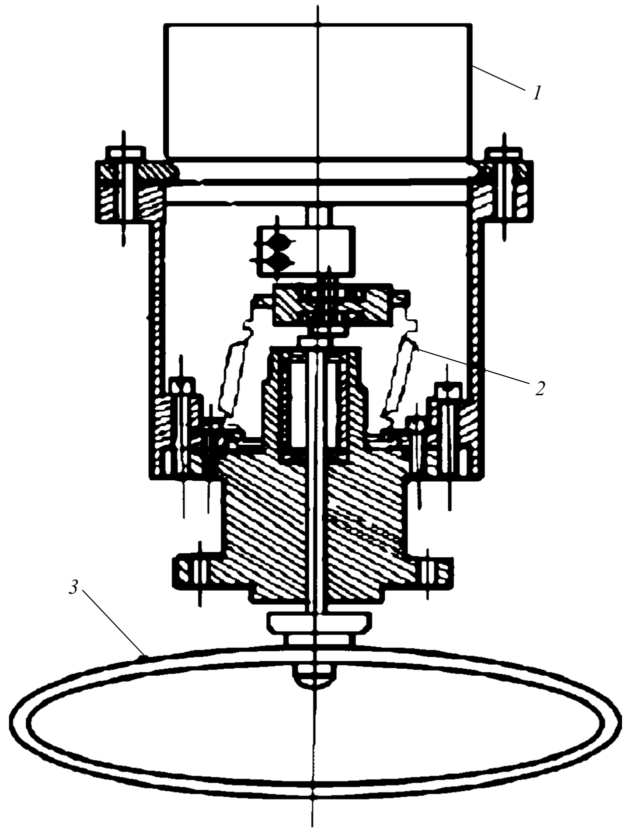

Figure 13. Frequency tuning unit: *1* — stepper motor, *2* — bellows, and *3* — ring.

A significant drawback of the H cavity is a decrease in the acceleration rate with increasing particle velocity. This is due to the fact that the voltage across the inner tube gap is constant along the cavity. This decrease in the acceleration rate can be slowed by increasing the voltage across the axially symmetric half of the double gap from the beginning to the end of the cavity, while maintaining the voltage across the quadrupole half.

To vary the voltage ratio across the halves of the double gap, it is necessary to vary the ratio of their capacitances and set the intermediate electrode legs at appropriate angles relative to the vertical plane. This cannot be done in the H cavity, since it is impossible to provide orthogonal field lines to the intermediate electrode legs. This drawback is eliminated in SH cavities [46] and 2Ch cavities [47].

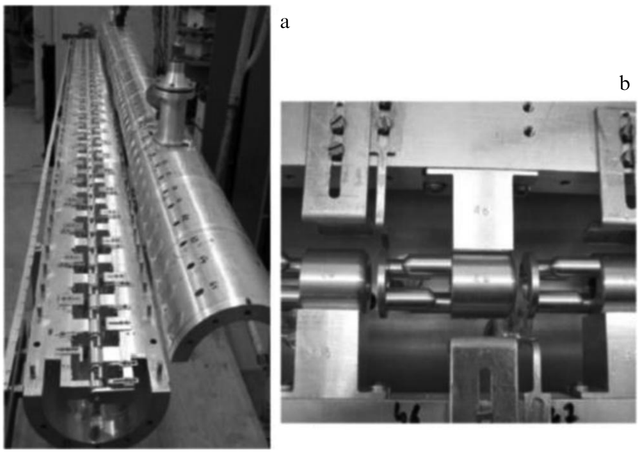

Figure 14. (a) Accelerating structure and (b) acceleration period with tuning elements.

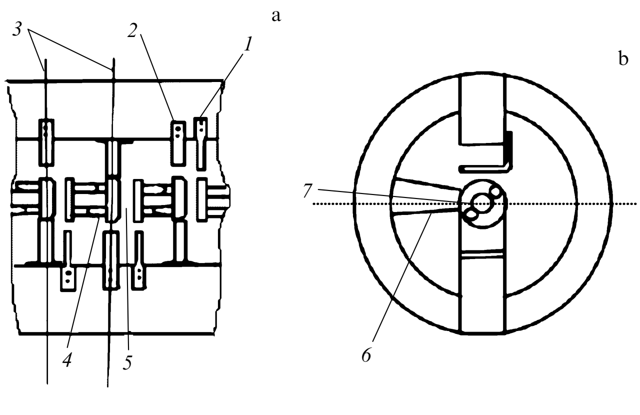

Figure 16. Acceleration period with tuning elements: (a) top view of acceleration channel and (b) view along channel axis: *1* — division ratio adjustment, *2* — frequency tuning, *3* — magnetic walls, *4* — focusing gap, *5* — accelerating gap, *6* — leg, and *7* — leg installation angle α.

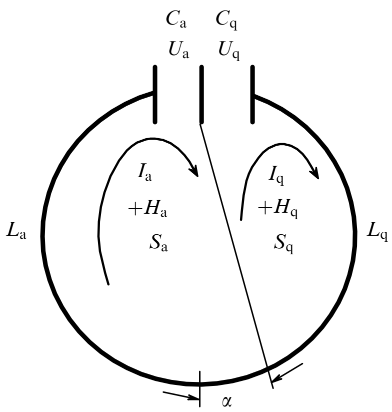

Figure 15. Schematic of capacitive divider formed by acceleration period electrodes. Subscript a corresponds to axially symmetric gap, and subscript q corresponds to quadrupole gap.

5.2 SH cavity and 2Ch cavity

These cavities have a sector-shaped cross section (Figs 10b and 10c), with the apex of the sector located on the axis of the accelerating channel; in this case, the orthogonality condition is satisfied automatically. They have lower RF power losses and a higher shunt resistance (in a 2Ch cavity, it is higher than in an SH cavity). Furthermore, in a 2Ch cavity, the tuning elements are moved to the sides of the resonator (Fig. 14b), which significantly simplifies adjustment of the acceleration period capacitances.

With changing voltage across the accelerating gap, the main problem is to determine the intermediate electrode leg angle in accordance with the specified voltage division in the double gap. A special technique was developed to determine this angle.

The acceleration period of the structure with SPQF is a capacitive voltage divider between the board electrodes (Fig. 15).

In the absence of current across the intermediate electrode leg, the relationship

$$\frac{U_a}{U_q} = \frac{C_q}{C_a} = \frac{\int_0^{S_a} \mu H_a \, dS}{\int_0^{S_q} \mu H_q \, dS} \qquad (14)$$

is met. It follows that the voltage division ratio U_a/U_q is determined by the ratio of the gap capacitances C_a/C_q, the areas S_a and S_q (i.e., the position of the intermediate electrode leg), and the magnetic fields H_a and H_q.

Calculating the capacitances C_a and C_q is a challenging task; estimates have shown that it easier to use the averaged magnetic fields H_a and H_q. The leg installation angle (α in Fig. 15) was precisely calculated using HFSS 3D simulation software.

The following sequence of actions was used [48]. A section of the cavity corresponding to the acceleration period was selected, bounded by 'magnetic walls' with the boundary conditions $E_\tau \neq 0$, $E_n = 0$, $H_\tau = 0$, $H_n \neq 0$ (Fig. 16).

Then, the distribution of the longitudinal field component E_z was integrated along a line coinciding with the focusing horn axis, yielding the desired values of U_a, U_q, as well as the dependences of U_a/U_q on the angle α. The resulting dependences were verified and refined using a model of the acceleration period. For this purpose, the end of the leg was disconnected from the resonator wall, and the voltage in the resulting gap was measured. A zero voltage indicated that the capacitance balance was achieved.

5.3 Calculation programs

More or less efficient programs for computer calculations of the electrodynamic characteristics of cavities for HFQF-based accelerators were not immediately available at the IHEP. Therefore, various model representations of electromagnetic fields in cavities had to be used.

One approach to solving this problem was to combine solutions in partial regions of the cavity (where there are no accelerating electrodes) with boundary conditions adopted from the assumption that the accelerating channel represents an electrostatic complex load for the equivalent circuits of these regions [43, 44, 51].

Electrodynamic parameters of cavities were first calculated using 2D solver programs such as SUPERFISH [49] and PRUD0 [50, 52]. They made it possible to numerically determine such important characteristics of H-wave cavities as the geometric dimensions of the cross section, the eigenfrequency of the operating oscillation, the quality factor, the effective shunt resistance, and the dissipative power losses, as well as to obtain an understanding of the transverse topography of the electromagnetic field.

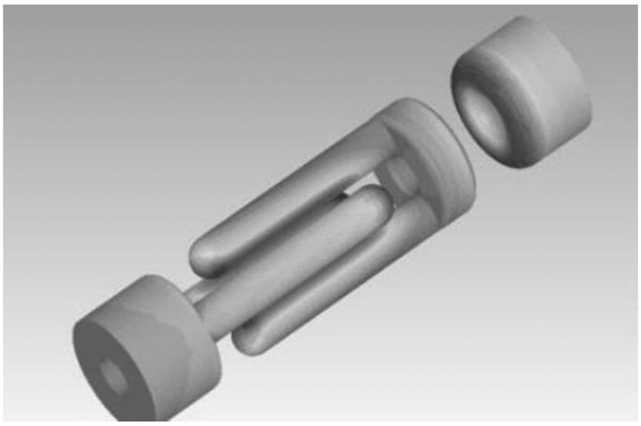

Figure 17. Field strength distribution on electrode surface (shown by electrode color intensity).

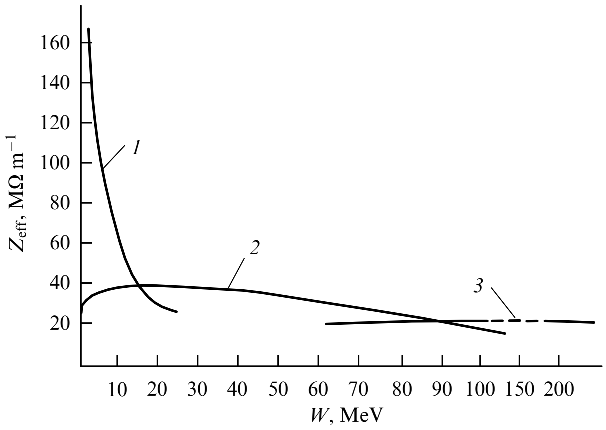

Figure 18. Effective shunt resistance as a function of energy for various structures: *1* — SPQF, *2* — Alvarez accelerator, and *3* — coupled cells.

Even the first 3D programs (MWS, HFSS), while still limited in their capabilities, began to provide significantly more information about the electrodynamic parameters of cavities than did 2D solver programs. Thus, HFSS software [48] not only facilitated the adjustment of the double gap in the 2Ch cavity but also made it possible to obtain the field strength distribution in the accelerating channel and determine the maximum field strength at the accelerating electrodes (Fig. 17).

Modern computers are incomparably more powerful than those from years ago. They can be used not only to calculate and adjust individual acceleration periods, but also to estimate and optimize the entire accelerator in terms of beam quality, manufacturability, cost, reliability, and efficiency.

5.4 Accelerator economic efficiency

The economic efficiency of an accelerator directly depends on the effective shunt resistance $Z_{\rm eff}$ of its accelerating system. Estimates of the dependence of $Z_{\rm eff}$ on particle energy, based on the data available at that time, showed that a proton accelerator with SPQF is more economic efficient than an Alvarez accelerator, up to $W_{\rm p} \approx 18$ MeV (Fig. 18).

Belyaev et al. [53, 54] made an attempt to predict the potential effective shunt resistance of a 2Ch cavity if it is optimized with respect to this parameter. According to these estimates, it can exceed the shunt resistance of an Alvarez resonator up to $W_{\rm p} \sim (30-40)$ MeV. This means that, in the energy range of interest for practical applications, it is possible to construct an HILA with HFQF that is more economic efficient than a conventional HILA.

5.5 Technological solutions

• **Resonator Materials.** Steel was used as the primary material for the first accelerating systems with SPQF. Steel is susceptible to corrosion, and so water with corrosion inhibitors was used in the cavity cooling channels. At that time (the 1970s), this was the simplest solution. The URAL-30 accelerator, developed using this technology, has been operating at the IHEP accelerator complex for 40 years. The URAL-30M, which will replace the URAL-30 accelerator, relies on the use of the AMg-6 alloy instead of steel, because the former has a number of valuable properties. They include high corrosion resistance, good machinability, low gas emission, good weldability, dimensional stability over time, sufficient strength, low specific weight, and, finally, good adhesion when applying galvanic copper ($\sim$ 100 μm).

• **Fabrication of accelerating electrodes.** The accelerating electrodes are made of MOb oxygen-free copper (the Mob grade is superior to other grades in terms of the electrical strength of the accelerating gaps). The focusing horns were welded to the electrodes using electron beam welding in a vacuum. Experiments were performed with horns welded to the electrode body using diffusion welding. Long horns were pressed into the electrode body. The joint was laser-welded to improve electrical contact. However, when straightening the horns, the welds failed, and laser welding was no longer used. A technology for manufacturing solid electrodes on machines with special tooling and software control was also employed. This technology ensures the best electrode quality.

• **Electrode alignment.** The URAL-30 (and URAL-30M) focusing channel consists of four sections. The inner tube of each section is divided into subsections (cavities) approximately 600 − 900 mm long, convenient for open-mounting the electrodes and subsequent installation of the cavities into the container.

The focusing channel should not contain any adjustment devices comparable in size to the electrodes. Therefore, a special test facility was made for mounting electrodes in the URAL-30 accelerator [55].

The cavity is positioned on the mounting test facility so that the accelerator axis coincides with the microtelescope axis, which is parallel to the base guide and the reference tape. The electrode is placed on the aperture target and secured in a holder on the base guide. The installation accuracy is better than 20 μm, and so only the longitudinal coordinate needs to be adjusted. Using two pentaprisms, the image of the electrode end and the reference tape is transmitted to the microtelescope. After installing the electrode, a bracket or rod of the intermediate electrode is secured to the cavity so that the electrode leg fits inside the cavity of the bracket (rod) without touching the walls. The cavity is heated to $\sim$ 100°C and filled with low-shrinkage solder (Wood's alloy). The cavities are then mounted in a container.

This method for mounting electrodes has stood the test of time. However, with the advent of computer-controlled, precision machines, it is no longer used at the IHEP. A method was developed for mounting electrodes directly using machines. The electrode leg seat is machined to the required precision using a microtelescope for control (Fig. 19).

Figure 19. Mounting of accelerating electrodes using a machine.

In Figure 19, the microtelescope is visible on the rear panel. Electrical contact between the leg and the cavity is ensured by an indium gasket. Compared to the previous mounting method, the reliability of electrode attachment has been improved, while the installation accuracy has been maintained. The electrodes in the URAL-30M accelerator were mounted using this method.

• **Tolerances for accuracy of HFQF channel parameters.** A focusing channel with HFQF and a channel with magnetic quadrupole lenses, having identical focusing and acceleration parameters, should have approximately the same tolerances for the accuracy of their parameter.

The problem of tolerances in HFQF-based accelerators was analyzed in detail in a number of studies [13, 56–59]. These studies utilized both analytical research methods and numerical simulations of particle dynamics. The consequences of specific manufacturing errors in the focusing channel elements and errors in its adjustment were determined.

The following tolerance system was adopted for the HFQF-based accelerators developed at the IHEP: root-mean-square errors of the longitudinal size of the channel elements, $\leqslant 0.06\%$ (as a fraction of $\beta\lambda$); deviations of the transverse size from the standard values, $\leqslant 50$ μm; error in the azimuthal position of the horns, $\leqslant 30'$; tolerance for the deviation of the gradient of the focusing field component from the nominal value, $\leqslant 1\%$; and tolerance for the RF field level in the section, $\leqslant 1\%$.

• **Thermal stabilization of cavities.** In order to maintain the adopted tolerance system during accelerator operation, the accelerator cavities must be thermally stabilized. This problem was studied both theoretically and by testing various cavity cooling models using a special test facility [60, 61].

The problem was theoretically solved using the finite element method in three stages. First, the distribution of dissipative RF power losses was calculated using the SUPERFISH program [49]. Then, using the obtained heat fluxes and taking into account the boundary conditions of heat transfer, the heat conductivity problem was solved, the results of which served as the initial data for the thermoelasticity problem. This calculation method is the basis of the HAST software package developed at the IHEP [60].

On the basis of calculations and experiments, the optimal thermal stabilization regime for the URAL-30M accelerator was determined: the water temperature in the cooling system is $(21 \pm 0.25)\,^{\circ}$C, the water flow rate through one channel is (0.015 ± 0.005) l s^{-1}, and the total water flow rate in the accelerator is (45–65) l min^{-1}. The displacements of the accelerator elements are within the range of ~ 15 μm.

• **Vacuum.** The use of the vacuum-melted AMg-6 alloy for the cavities and containers, vacuum-tight galvanic copper plating of the conductive surfaces, and indium seals allowed us to achieve a vacuum of at least 10^{-8} Torr in the HFQF-based accelerating system. In this case, use was made of a relatively small number of NMD-0.16 vacuum pumps. Furthermore, additional getter pumps, which maintained the forevacuum in the accelerator during shutdowns, were of great help.

6. RF power supply system

A distinctive feature of the accelerating systems used for accelerators with HFQF is their small size: for the same wavelength, the diameters of the H-wave cavities are three-to-four times smaller than the diameter of the Alvarez cavity. Consequently, for the same field strength, the stored energy is an order of magnitude lower. Due to the low stored energy, when the accelerated particle beam is turned on, there is a rapid field 'upsurge' in the cavity of an accelerator with HFQF. The issue of field upsurge compensation in accelerators with HFQF has received special attention.

6.1 Automatic compensation system

An original system for automatic compensation of the power used for particle acceleration was proposed at the IHEP, namely, the AC system [62–69] (Fig. 20). It uses the voltage wave reflected from the cavity as a feedback signal to control excitation of the final stage amplifier (FSA).

The system provides distributed power input via multiple coupling loops at a high power level. Power from the FSA is

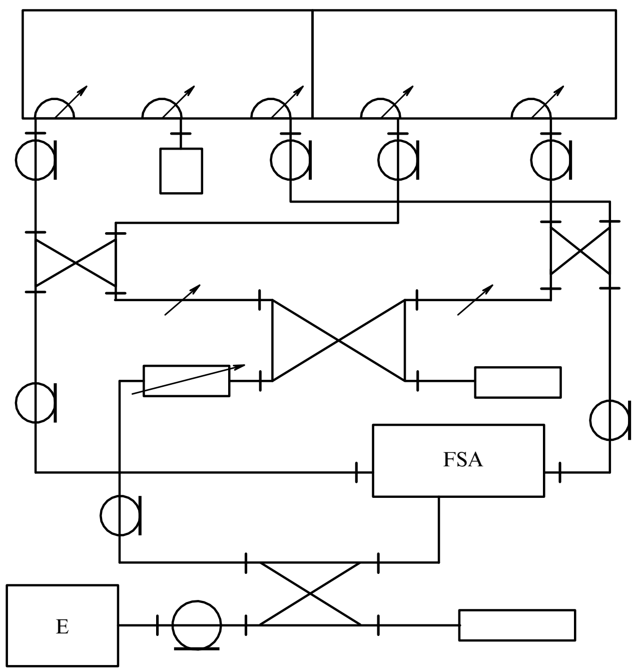

Figure 20. Schematic of AC system.

fed into two cavity sections via a double T-bridge. The cavity sections have equal reflectances and RF field phases shifted by $\pi/2$. The sections are designed with identical particle energy gains and identical shunt resistances, adjustable using a ballast load. With identical beam load changes in the sections, the power reflected from them is released in the decoupled arms of the first T-bridge and in the ballast load. Part of the power through the second T-bridge is summed in the desired phase with the exciter (E) power and fed as a control signal to the FSA.

The AC system functions as a ferrite Y-circulator introducing active losses into the system when the oscillator and cavity are mismatched. At that time, megawatt-power circulators had not yet been developed, and the AC system, made using available technology, was not reliable enough and was eventually abandoned. However, with modern components, the AC system has the potential for development: it is built on passive elements and provides a high-speed response with complete compensation for the RF field amplitude and phase disturbances, regardless of the amplifier gain.

6.2 RF power supply system of URAL-30M accelerator

The URAL-30M accelerator has a classic RF power supply circuit with branching at low power levels. To achieve the specified RF field amplitude and phase stability of $\sim (\pm 1\%)$, an automatic amplitude and phase control system was developed.

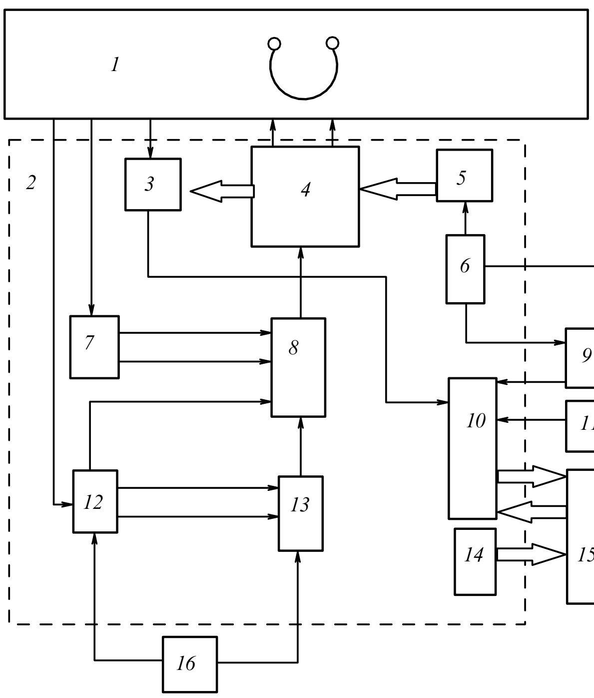

Figure 21. Simplified schematic of RF power supply system channel: *1* — accelerator section; *2* — RF power supply system channel; *3* — breakdown protection unit; *4* — RF power amplification channel; *5* — anode voltage modulator; *6* — secondary power supply units; *7* — amplitude stabilization system; *8* — attenuator–phase shifter module; *9* — vacuum system of accelerator sections; *10* — control, interlock, and signaling circuit units; *11* — water cooling system; *12* — phase stabilization system; *13* — electronic phase shifter unit; *14* — measurement system; *15* — automated accelerator measurement and control system; and *16* — driver.

The URAL-30M RF power supply system consists of five identical RF power supply channels. One of them is shown in Fig. 21.

Systems such as the driver and primary power supply system are common to all five channels. Beam current sensors are installed between the sections.

The amplitude of the accelerating field in the accelerator cavity is stabilized relative to the reference voltage by regulating the output power of the amplification channel by varying the excitation at its input while maintaining a constant anode voltage. The amplitude stabilization system contains three channels that offer control based on deviation from the reference voltage, beam field disturbance (a signal received from the beam current sensor), and a program implemented using a signal synchronized with the accelerator timer.

The elements of the phase automatic control system (ACS) are identical to the corresponding elements of the amplitude ACS in design, function, and requirements.

The development of anode voltage modulators for vacuum-tube RF stages is based on a modular principle, which has the following advantage: it allows a set of individual modules to implement the parameters required for specific equipment operating conditions. Moreover, it eliminates the need for regulated power supplies, significantly simplifying the equipment.

Each power amplification channel is equipped with a breakdown protection unit. Random breakdowns of the interelectrode gaps occur in a statistically negligible percentage of the total number of pulses. Typically, they do not happen in more than two consecutive pulses and are not a sign of a pre-emergency state. Conversely, breakdowns occurring in a continuous series of pulses indicate an impending emergency. Therefore, when there is a series of breakdowns, the breakdown protection unit quickly turns off the anode voltage modulator of the corresponding RF channel. The operator is then able to understand the causes of the pre-emergency situation.

7. Commissioning and operation of accelerators with high-frequency quadrupole focusing

Commissioning and operating an accelerator with SPQF can be assessed based on the experience of startup and operation of the URAL-30 accelerator.

URAL-30 consists of a front end of an accelerator with SHQF and two sections of the main part of an accelerator with SPQF. Each section is divided into two subsections with the same energy gain for accelerated particles (a prerequisite for implementing the AC system). In other words, the accelerator essentially consists of five sections, each with its own individual configuration.

One of the tasks during the startup of a linear accelerator is to determine the threshold and nominal levels of the RF fields in the accelerator sections. The RF field in an accelerator with HFQF simultaneously accelerates and focuses particles; therefore, when studying the first sections, subsequent sections must be turned off. However, this leads to a significant loss of the beam on the way to the measuring devices and complicates the mutual configuration of the sections. Nevertheless, it is possible to determine threshold levels in all sections due to the fact that beam focusing by the RF field begins earlier than resonant acceleration.

In the initial part of the accelerator (in the RFQ), the threshold was determined using the following method [70]. All sections except the RFQ were completely switched off. The beam with the RFQ energy at the accelerator channel output was deflected using a magnetic analyzer (MA) onto a Faraday cup (FC) coated with a phosphor. The width of the energy spectrum was estimated from the size of the spot on the phosphor. The dependence of the spectrum width and its position on the phosphor on the field level in the RFQ was determined. The threshold was assessed by the moment of shift and disappearance of the spectrum.

When determining the threshold in the first subsection of the first section of the main part of the accelerator (MPA) (C_{1-1}), all subsequent sections were switched off, and the RF field levels in the RFQ and C_{1-1} were set to levels close to the calculated nominal values. The magnetic analyzer was tuned to the C_{1-1} energy. Using the maximum current in the MA, the optimal phase difference of the RF field between the C_{1-1} and the RFQ was selected, and the position of the spectrum center on the FC was recorded. The dependence of the spectral center shift on the RF field level in C_{1-1} was then plotted. The threshold was estimated by the disappearance of the phosphor glow.

The RF field threshold levels in the remaining sections of the MPA were determined in the same way as in the C_{1-1}. Nominal levels were set based on the threshold values and then refined based on the spectrum width at the accelerator output (at nominal levels, it is the narrowest and most stable).

Monitoring X-rays from the surface of the accelerating electrodes, as well as radiation associated with particle losses, also proved useful for adjusting the URAL-30 accelerator [71, 72]. X-ray radiation was measured using high-speed scintillation counters, counters with photomultiplier tubes, and ionization chambers. Neutron radiation was monitored using a neutron detector based on a helium ionization chamber and rhodium and indium activation detectors.

The operation of the URAL-30 accelerator includes typical tasks for any ion linear accelerator: maintaining the specified operating regimes of the accelerator during beam-consuming operations and performing equipment maintenance between operations.

8. Conclusions

Let us draw some conclusions.

Ion linear accelerators with HFQF (comprising SHQF and SPQF), both in the proton version in a certain energy range and for accelerating heavy ions, may be preferable for use.

The technologies mastered at the IHEP in developing HFQF-based accelerators do not contain anything exotic. Undoubtedly, the use of modern technologies will allow the HFQF problems mentioned in the paper to be solved more easily and at a higher quality level.

The technologies developed for proton accelerators with HFQF can be used to fabricate HILAs with HFQF. Such accelerators may prove to be very promising for producing accelerated heavy ion beams, which are necessary for many practical applications. These accelerators can be both inexpensive and cost-effective, which is important for an industrial accelerator. When used as an injector for a ring accelerator, they provide a high-quality beam for injection.

Like SHQF, SPQF has proven its performance in practice over decades.

Acknowledgments. The authors consider it their duty to honor the memory of the untimely deceased IHEP researchers who made a decisive contribution to the development and fabrication of linear accelerators with HFQF. They include O.K. Belyaev, V.B. Stepanov, O.V. Ershov, I.G. Mal'tsev, E.V. Mazurov, and A.V. Zherebtsov. V.A. Teplyakov, the founder of the high-frequency quadrupole focusing system and the longtime leader of our team, played a particularly outstanding role.

References

1. Belyaev O K et al. *Phys. Part. Nucl. Lett.* **10** 795 (2013); *Pis'ma Fiz. Elem. Chast. Atom. Yad.* **10** 1292 (2013)
2. Vladimirskii V V *Prib. Tekh. Eksp.* (3) 36 (1956)
3. Karetnikov D V et al. *Lineinye Uskoriteli Ionov* (Ion Linear Accelerators) (Moscow: Gosatomizdat, 1962) p. 71
4. Fer F et al., in *Trudy Mezhdunarod. Konf. po Uskoritelyam, Dubna, 21–27 Avgusta 1963 g.* (Proc. of the Intern. Conf. on Accelerators, Dubna, August 21–27, 1963) (Eds A A Kolomenskii et al.) (Moscow: Atomizdat, 1964) p. 513
5. Mal'tsev A P, Teplyakov V A *Prib. Tekh. Eksp.* (4) 29 (1965)
6. Boussard D, in *Proc. of the 1st Particle Accelerators Conf., 10–12 March 1965, Washington, DC, USA*; *IEEE Trans. Nucl. Sci.* **12** 648 (1965)
7. Mal'tsev A P, Zotova E A, Teplyakov V A *Prib. Tekh. Eksp.* (4) 20 (1964)
8. Teplyakov V A et al. *Prib. Tekh. Eksp.* (4) 26 (1965)
9. Teplyakov V A et al. *Prib. Tekh. Eksp.* (6) 24 (1964)
10. Mal'tsev A P, Ermakov S M, Teplyakov V A *Atom. Energy* **23** 917 (1967); *Atom. Energ.* **23** (3) 195 (1967)
11. Teplyakov V A, Stepanov V B *Radiotekh. Elektron.* **1** 1965 (1968)
12. Teplyakov V A et al. *Byull. Izobret.* (19) 93 (1967)
13. Mal'tsev A P, Stepanov V B, Teplyakov V A, Preprint No. 69-2 (Serpukhov: IHEP, 1969)
14. Il'evskii S A et al. *Atom. Energy* **34** 77 (1973); *Atom. Energ.* **34** (1) 56 (1973)
15. Kapchinskii I M, Teplyakov V A *Prib. Tekh. Eksp.* (2) 19 (1970)
16. Kapchinskii I M, Teplyakov V A *Prib. Tekh. Eksp.* (4) (1970)
17. Mal'tsev A P, Stepanov V B, Teplyakov V A, Preprint No. 71-116 (Serpukhov: IHEP, 1971)
18. Kapchinskii I M, Preprint No. 72-29 (Serpukhov: IHEP, 1972)
19. Kapchinskii I M, Mal'tsev A P, Teplyakov V A, in *Trudy VII Mezhdunarod. Konf. po Uskoritelyam Chastits Vysokikh Energii, Erevan–Tsakhkadzor, 1969 g.* (Proc. VII Intern. Conf. on High-Energy Particle Accelerators, Yerevan–Tsakhkadzor, 1969) Vol. 1 (Erevan: Izd. AN ArmSSR, 1970) p. 153
20. Vladimirskii V V, Kapchinskii I M, Teplyakov V A *Byull. Izobret.* (10) 75 (1970)
21. Golosai N I et al. *Atom. Energy* **39** 716 (1975); *Atom. Energ.* **39** (2) 123 (1975)
22. Ioffe B L et al., in *Trudy VI Vsesoyuz. Soveshchaniya po Uskoritelyam Zaryazhennykh Chastits, Dubna 11–13 Oktyabrya 1978 g.* (Proc. VI All-Union Conf. on Charged Particle Accelerators, Dubna, October 11–13, 1978) Vol. 1 (JINR Publications, D9-11874) (Dubna: JINR, 1979) p. 236
23. Potter J M et al., in *Proc. of the 8th Particle Accelerators Conf., PAC'79, San Francisco, CA, USA, 12–14 March 1979*; *IEEE Trans. Nucl. Sci.* **26** 3745 (1979)
24. Ado Yu M et al., in *Trudy V Vsesoyuz. Soveshchaniya po Uskoritelyam Zaryazhennykh Chastits, Dubna, 5–7 Oktyabrya 1976 g.* (Proc. V All-Union Conf. on Charged Particle Accelerators, Dubna, October 5–7, 1976) Vol. 1 (Moscow: Nauka, 1977) p. 42
25. Gorshkov B M et al. *Sov. Phys. Tech. Phys.* **22** 1348 (1977); *Zh. Tekh. Fiz.* **47** 2328 (1977)
26. Egorov A A et al. *Sov. Phys. Tech. Phys.* **26** 942 (1981); *Zh. Tekh. Fiz.* **51** 1643 (1981)
27. Zherebtsov A V, Mal'tsev A P, Teplyakov V A, Preprint No. 90-29 (Protvino: IHEP, 1990)
28. Zenin V A et al., in *Trudy VIII Vsesoyuz. Soveshchaniya po Uskoritelyam Zaryazhennykh Chastits, Protvino, 19–21 Oktyabrya 1982 g.* (Proc. VIII All-Union Conf. on Charged Particle Accel-

erators, October 19–21, Protvino, 1982) Vol. 2 (Dubna: JINR, 1983) p. 77
29. Zenin V A et al., in *Trudy XIII Mezhdunarodnoi Konf. po Uskoritelyam Zaryazhennykh Chastits, Novosibirsk, 7–11 Avgusta 1987 g.* T.1) (Proc. XIII Intern. Conf. on Charged Particle Accelerators, Novosibirsk, August 7–1, 1987) Vol. 1 (Ed. A N Skrinskii) (Novosibirsk: Nauka, 1987) p. 312
30. Demikhovsky D A et al., in *Proc. of the 1st European Particle Accelerator Conf., EPAC 1988, Rome, Italy, 7–11 June 1988* Vol. 1 (Ed. S Tazzari) (Singapore: World Scientific, 1989) p. 605
31. Zenin V A et al., Preprint No 93-147 (Protvino: IHEP, 1993)
32. Belyaev O K et al., in *Proc. of the 20th Russian Conf. on Charged Particle Accelerators, RuPAC 2006, Novosibirsk, Russia, September 10–14, 2006* (Eds M Kuzin, E Shirkova) (Novosibirsk: BINP, 2006) p. 273
33. Konoplev E A, Mal'tsev A P, Stepanov V B, Preprint No. 72-24 (Serpukhov: IHEP, 1972)
34. Dernovoi G N, Mal'tsev A P *Zh. Tekh. Fiz.* **52** 1209 (1982)
35. Budanov Yu A, Mal'tsev A P, Preprint No. 83-9 (Serpukhov: IHEP, 1983)
36. Stepanov V B, Teplyakov V A *Byull. Izobret.* (13) 226 (1970)
37. Timofeev A A, Patent RF for Invention 24561130 (2012)
38. Protas'ev V B, Timofeev A A, Preprint No. 2009-3 (Protvino: IHEP, 2009)
39. Dernovoi G N et al., Preprint No. 75-1 (Serpukhov: IHEP, 1975)
40. Zherebtsov A V, Mal'tsev A P, Preprint No. 80-47 (Serpukhov: IHEP, 1980)
41. Teplyakov V A, Mal'tsev A P, Stepanov V B, Preprint No. 2006-5 (Protvino: IHEP, 2006)
42. Kilpatrick W D *Rev. Sci. Instrum.* **28** 824 (1957)
43. Stepanov V B, Teplyakov V A, Preprint No. 74-130 (Serpukhov: IHEP, 1974)
44. Stepanov V B, Preprint No. 74-151 (Serpukhov: IHEP, 1974)
45. Belyaev O K, Preprint No. 2011-10 (Protvino: IHEP, 2011)
46. Belyaev O K, Ryabov A D, Stepanov V B *Prib. Tekh. Eksp.* (5) 96 (1998)
47. Belyaev O K et al., Preprint No. 92-58 (Protvino: IHEP, 1992)
48. Belyaev O K, Zvonarev I A *Instrum. Exp. Tech.* **53** 327 (2010); *Prib. Tekh. Eksp.* (3) 13 (2010)
49. Daikovskii A G, Portugalov Yu I, Ryabov A D, Preprint No. 80-107 (Serpukhov: IHEP, 1980)
50. Barsukov A B et al., Preprint No. 82-178 (Serpukhov: IHEP, 1982)
51. Barsukov A B, Preprint No. 80-163 (Serpukhov: IHEP, 1986)
52. Abramov A G et al., in *Trudy VIII Vsesoyuz. Soveshchaniya po Uskoritelyam Zaryazhennykh Chastits, Protvino, 19–21 Oktyabrya 1982 g.* (Proc. VIII All-Union Conf. on Charged Particle Accelerators, Protvino, October 19–21, 1982) Vol. 1 (Dubna: JINR, 1983) p. 149
53. Belyaev O K et al., Preprint No. 90-125 (Protvino: IHEP, 1990)
54. Belyaev O K, Stepanov V B, Preprint No. 87-135 (Protvino: IHEP, 1987)
55. Stepanov V B et al. *Prib. Tekh. Eksp.* (6) 20 (1972)
56. Mal'tsev A P *Atom. Energy* **21** 963 (1966); *Atom. Energ.* **21** (4) 295 (1966)
57. Mal'tsev A P, Shulaev G A *Zh. Tekh. Fiz.* **52** 1604 (1982)
58. Shulaev G A, Preprint No. 89-115 (Serpukhov: IHEP, 1989)
59. Barsukov A B, Belyaev O K, Igoshin V B, Preprint No. 84-16 (Serpukhov: IHEP, 1984)
60. Abramov A G et al., Preprint No. 84-64 (Serpukhov: IHEP, 1984)
61. Grushichev I A, Popovkin V V, Preprint No. 92-141 (Protvino: IHEP, 1992)
62. Mal'tsev I G, Teplyakov V A, Preprint No. 74-112 (Serpukhov: IHEP, 1974)
63. Teplyakov V A *Byull. Izobret.* (41) 160 (1974)
64. Mal'tsev I G, Teplyakov V A *Byull. Izobret.* (5) 211 (1976)
65. Mal'tsev I G, Teplyakov V A, Preprint No. 76-137 (Serpukhov: IHEP, 1976)
66. Mazurov E V, Mal'tsev I G, Nagaev V I, Preprint No. 77-122 (Serpukhov: IHEP, 1977)
67. Mal'tsev I G, Preprint No. 80-4 (Serpukhov: IHEP, 1980)
68. Mazurov E V, Mal'tsev I G, Nagaev V I, Preprint No. 81-125 (Serpukhov: IHEP, 1981)
69. Mal'tsev I G, Teplyakov V A, Preprint No. 74-112 (Serpukhov: IHEP, 1974)
70. Zenin V A, Preprint No. 82-160 (Serpukhov: IHEP, 1982)
71. Zenin V A, Chimankov M N, Preprint No. 85-103 (Serpukhov: IHEP, 1985)
72. Zenin V A et al., Preprint No. 85-177 (Serpukhov: IHEP, 1985)